Journal of Structural Geology, Vol. 9, No. 5/6, pp. 667 to 677, 1987
Printed in Great Britain

0191-8141/87 $03.00 + 0.00

Computer models of pressure shadows: a method for strain measurement and shear-sense determination

A. ETCHECOPAR and J. MALAVIEILLE

Laboratoire de Géologie Structurale, U.A. 266, Université des Sciences et Techniques du Languedoc, Place Eugène Bataillon, 34060 Montpellier Cédex, France

(*Received* 5 *March* 1986; *accepted in revised form* 2 *March* 1987)

Abstract—In this paper a computer model of pressure-shadow growth is presented based on a principle of geometrical best fit between a rigid object and a deformable matrix. By varying the parameters in the simulation, pressure shadows of different shapes can be generated and matched by trial-and-error with specific natural examples. Thus the method is able to give estimates of crystallization laws, finite strain and deformation path. Simulations carried out for a number of natural examples show that: (1) the pressure-shadow infilling material can be rigid or deformable and the direction of growth appears to be mostly 'displacement controlled'; (2) the finite strain is larger than what appears from the shape of the pressure shadow; and (3) the deformation path may be 'replayed' by the simulation. From the results of the simulations we emphasize the morphological characteristics of pressure-shadows which can be reliably used for shear-sense determination.

INTRODUCTION

FINITE-STRAIN analyses and kinematic reconstructions are of great value in the study of crustal deformation. During the last few decades, various methods for analyzing finite strain (recently reviewed by Ramsay & Huber 1983) and the sense and amount of rigid rotation (Simpson & Schmid 1983, Nicolas 1984) have been developed. None of these methods allows measurement of both finite strain and rotation. Furthermore, some methods of shear-sense determination appear to be conflicting and are still controversial.

We present a numerical method for simulating the development of pressure shadows. The results allow us to estimate the amount of deformation and rotation in natural examples. We use pressure shadows because they are common in metamorphic rocks, because they accurately record incremental strains, and because their geometry and their growth processes are well documented (Mügge 1928, 1930, Pabst 1931, Demay 1942, Fairbairn 1950, Frankel 1957, Langheinrich 1964, Zwart & Oele 1966, Ramsay 1967, Spry 1969, Choukroune 1971, Elliott 1972, Durney & Ramsay 1973, Subieta 1977, White & Wilson 1978, Malavieille *et al.* 1982, Malavieille & Etchecopar 1984). We have chosen a geometrical model for two reasons.

(1) The deformation path can be inferred only from the shape and the internal geometry of pressure shadows.

(2) The treatment of many samples is possible because the quality of the geometrical fit between actual and computed pressure shadows can be easily and quickly assessed by eye.

After a short review of the subject, we will explain the principles of our simulation, and then apply it to some actual examples from several well-known tectonic contexts.

PRESSURE SHADOW CHARACTERISTICS

A recent and complete review by Ramsay & Huber (1983) considers two main types of pressure shadows: *pyrite type* and *crinoid type*. In the crinoid type, progressive fibre growth occurs from the object surface towards the displaced matrix, with crystallographic continuity between fibres and object. This paper is concerned only with the more common pyrite type, (Fig. 1) where incremental crystalline growth of fibres is located at the interface between the object and its pressure shadow. According to the way fibres grow, we distinguish two categories: *displacement-controlled fibres*, with a consistent geometry of progressive growth of fibres from the wall towards the resistant object; and *face-controlled fibres*, with fibre axes growing normal to the face of the resistant crystal, irrespective of the displacement directions.

During deformation, fibres in pressure shadows may be *deformable* or *rigid*, depending on pressure and temperature conditions. High temperatures usually imply deformable pressure shadows with strong recrystallization. On the other hand, at low temperatures, pressure shadows are usually rigid and fibrous. Depending on whether the fibres are deformable or rigid, so they react differently to progressive deformation.

Some authors (e.g. Choukroune 1971, Ramsay & Huber 1983) have presented methods to determine incremental rotation and displacement of either the object with respect to the pressure shadow, or the pressure shadow with respect to the object. These methods do not account for the rotation of the whole association (object + pressure shadow) with respect to the matrix. In this paper we present a computer model for rotation and crystalline growth, controlled by the incremental deformation of the matrix (as in natural pressure shadows).

MODELS

General principles

We assume that pressure shadows result from the difference in deformation between a resistant object and a ductile matrix. For each increment of deformation, this mismatch induces gaps and boundary sliding. In the computer models we seek the rotation and translation of the object that minimize gaps and boundary sliding. Our method is basically that proposed by Etchecopar (1974, 1977, 1984) for the minimization of gaps, overlaps and boundary sliding between the various cells of a polycrystalline aggregate.

We first define the boundaries of the object (Fig. 3), using regularly spaced points $[O_i]$. For each increment of strain, we compute the theoretical polyhedron resulting from finite deformation of the object boundaries, assuming equal ductility between matrix and object. The original points $[O_i]$ thus occupy new positions $[M_i]$. We then compute the translation and the rotation of the rigid object which minimizes the squares of the distances $M_i - O_i$. This minimization reduces the amount of gaps and boundary sliding between object and matrix. The gaps which still remain are assumed to represent an incremental pressure shadow. In other words, the crystallization rate is assumed to be high enough in comparison with the strain rate to fill the remaining gap in a passive way. According to the behaviour of the material already crystallized, we distinguish two kinds of models, the *rigid-fibre model* and the *deformable-fibre model.*

Rigid-fibre model (*Fig.* 4). In this model, the pressure shadows which have already crystallized are rigid. Thus, the model, contains three separate rigid elements, the object itself and the two associated pressure shadows. Due to the high crystallization rate assumed at the surface of the original object, displacements at the interface between object and pressure shadows are unconstrained. Consequently, for the object as well as for the pressure shadows, minimization is performed only at the external boundaries between each of these rigid elements and the matrix (Fig. 4). Following this geometrical principle, we compute, for each increment and for each rigid element, the translation and the rotation that minimize gaps and boundary sliding. We also assume that the gap appearing between the former pressure shadow and rigid object is filled by new material. On the other hand, we assume that the gap appearing between the pressure shadow and matrix is not rigid, but as deformable as the matrix. We base this assumption on our observations of natural samples, which show that only minor crystallization develops on matrix boundaries of preexisting major pressure shadows (Fig. 2a).

Deformable-fibre model (Fig. 5). In this model, the pressure shadow and the matrix have the same ductility. So, for each new increment, the former pressure shadow and matrix deform in the same way and no gap appears between them. New crystallization occurs only between the rigid object and the already crystallized pressure shadow incorporated into the matrix.

In each of the two models described, it is possible to specify two modes of fibre growth, the *face-controlled* fibres and *displacement-controlled* fibres of Ramsay & Huber (1983). In the former, fibres grow orthogonally to the face of the crystal (Fig. 5); whereas, in the latter, fibres grow along the displacement path between the pressure shadow wall and the rigid object (Fig. 4).

Results

Initially identical configurations, containing square objects have been subjected to a deformation history of either pure shear or simple shear (Figs. 5–7). The models show the morphological characteristics of pressure shadows which are related to the imposed strain and rheological properties of the fibres. For simple shear (Figs. 5 and 6), note the asymmetry of pressure shadows, occurrence of asymmetric suture lines and formation of fibre domains of anomalous orientation, not in contact with the object. The simulations show that the direct measurement of pressure shadow lengths does not give the same amount of finite strain as that calculated from the superposed increments. The matrix strain ratio is approximately the square of the measured (X/Z) ratio of the pressure-shadow structures.

COMPARISON OF MODELS WITH NATURAL EXAMPLES

Method

We compare the computer models with XZ sections (cut perpendicular to cleavage and parallel to lineation) of naturally deformed specimens from geologically well-documented areas (Fig. 1). Samples contain pyrite crystals of various shapes and have undergone strains of various intensities. To model a natural example, one of the previously described crystallization mechanisms was chosen and then each of a number of parameters was varied until a best-fit result was obtained. The parameters varied were as follows: (1) initial orientation of the crystal with respect to the shear plane; (2) magnitude of incremental simple shear (γ_i), (3) magnitude of incremental shortening (K_{i1}); and (4) magnitude of incremental elongation (K_{i2}).

The transformation of a point (X, Y) into a point (X', Y') by variation of the above parameters is as follows:

$$X' = (X + Y\gamma_i)K_{i2},$$
$$Y' = YK_{i1}.$$

Example 1 (*Fig.* 8)

Geological features. The first sample (Fig. 8a) from southern Tibet (Mesozoic flysh, south of Yamdroktso), was slightly deformed at metamorphic conditions close to lower-greenschist facies (Burg *et al.* 1980). The

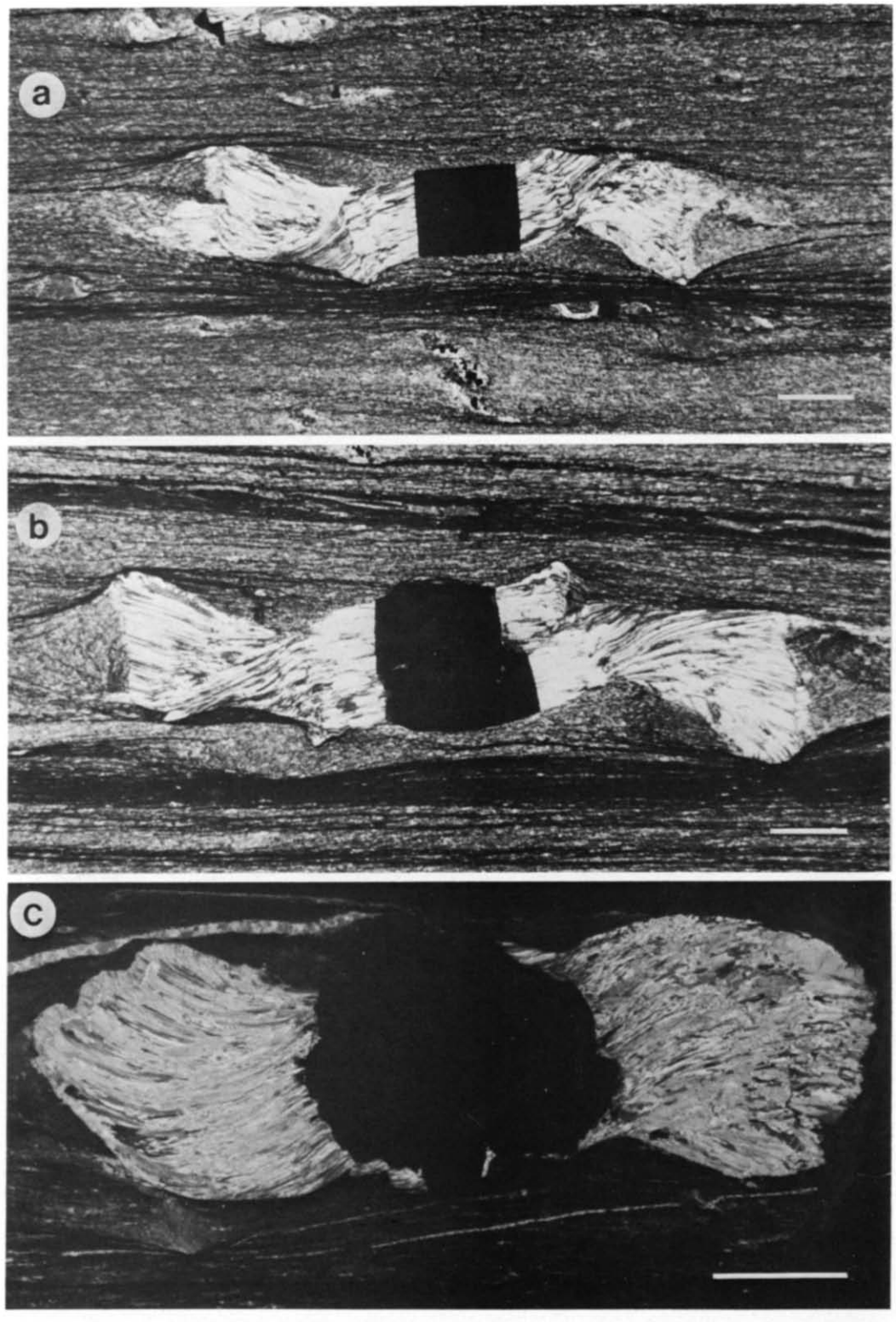

Fig. 1. Pressure shadows of (a) example 2, (b) example 3 and (c) example 4.

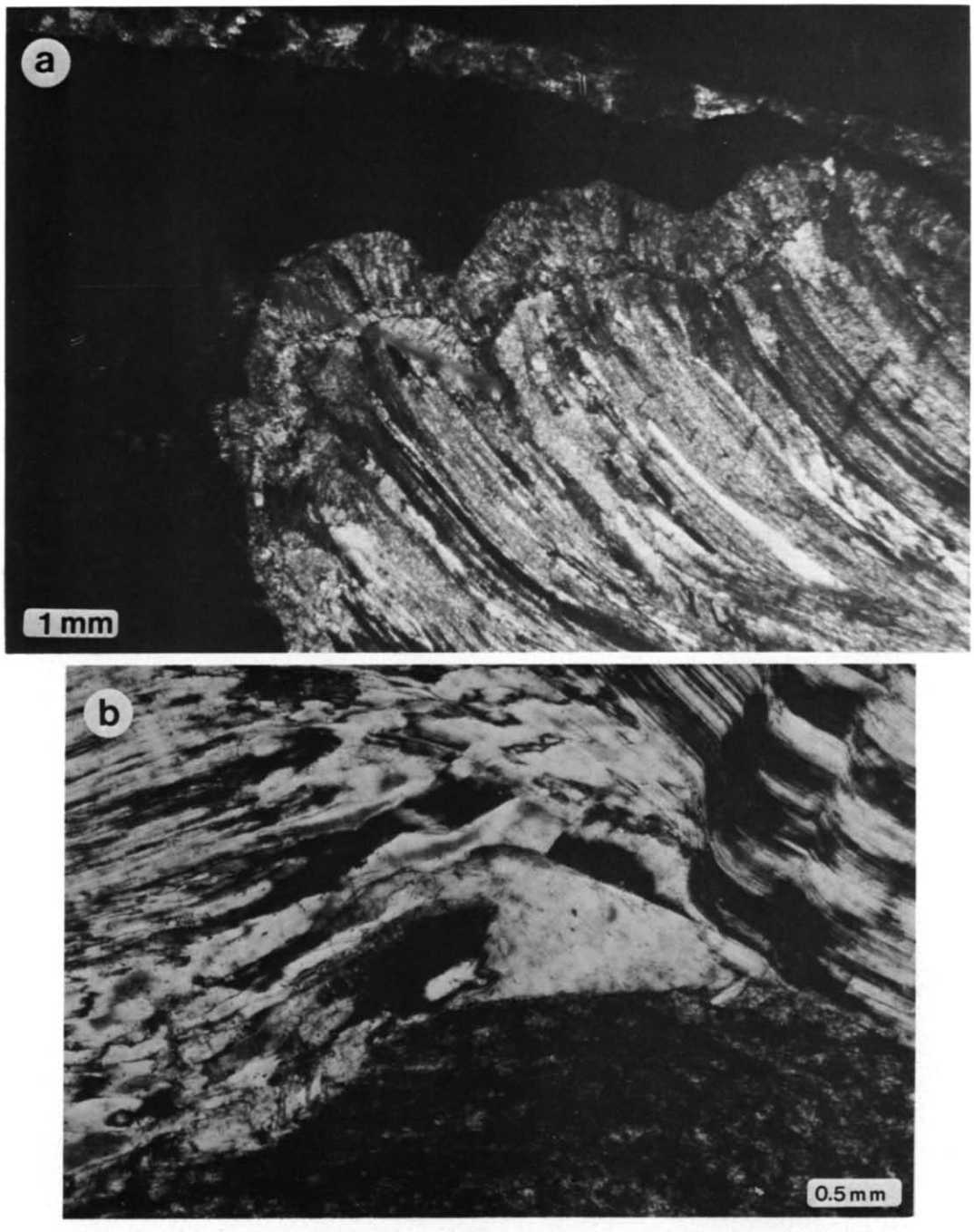

Fig. 2(a). Minor recrystallization developed at the top-left pressure shadow/matrix interface; example 4 (Fig. 1c). (b) Non-fibrous quartz crystals infilling a gap between a fibrous pressure shadow and its matrix; example 2 (Fig. 1a and Cover).

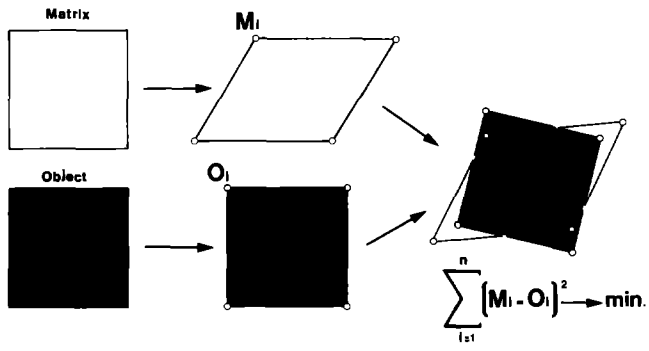

Fig. 3. General principle of the model (see text). The white square shows the initial shape of the object in the matrix. The black one represents the object itself. The white parallelepiped shows the deformation of the matrix (assuming equal ductility in matrix and in object). The black parallelepiped shows the deformed object (less deformable than matrix). The best fit is obtained by minimization of the squares of the difference $[M_i - O_i]$.

pressure shadows of this trapezoidal pyrite consist of quartz fibres. The pressure shadows and suture lines separating domains with differently orientated fibres are strongly asymmetric to cleavage.

The model. A best fit to Fig. 8(a) is derived from the following model parameters: (i) fibres are deformable and face-controlled; (ii) deformation is by progressive simple shear, with no additional shortening or elongation; (iii) simple shear increments are $\gamma_i = 0.1$ and total shear strain $\gamma_f = 1$. This simulation is shown in Fig. 8(b): a comparison with (a) would seem to verify the non-coaxial (simple shear) nature of strain in this example.

Examples 2 and 3 (Figs. 9 and 10)

Geological setting. Both these examples of pyrite pressure shadows come from the same outcrop in the French Pyrenees (Lourdes), where other samples have been studied by Choukroune (1971) and Ramsay & Huber (1983). The rectangular pyrite (Fig. 9a), and the one with a more complex shape (Fig. 10a), both shown in Fig. 1, have very asymmetric pressure shadows, made of quartz fibres. (Note that Fig. 1(a) is the 1987 cover photograph of this Journal.)

The model. A best fit has been obtained using rigid displacement-controlled fibres (Figs. 8b and 9b). The incremental strain parameters are: $\gamma_i = 0.2$, $K_{i1} = 0.98$, $K_{i2} = 1/0.98$ (plane strain). The finite-strain parameters are: $\gamma_f = 5$, $K_{f1} = 0.6$, $K_{f2} = 1.66$. Best fits for both pressure shadows were obtained by using the same laws and parameters. This indicates that the deformation which affected them was the same (i.e. homogeneous).

Figure 11 shows how small changes in the parameters can drastically modify the morphology of the model pressure shadows. Although the comparison of these model and natural examples is satisfactory, some details of the real pressure shadow still remain to be explained. There are two small domains of poorly oriented non-fibrous quartz crystals (Fig. 2b and 9a). These aggregates probably do not belong to the pressure shadow itself, but are the infill of a gap formed during rotation (Fig. 6a) between the fibrous complex and the matrix which cannot accommodate the very high deformation required in this particular zone. In the two examples (as in every other sample from this outcrop), two kinked domains within the pressure shadow can be observed which we ascribe to a significant, but brief, variation of incremental strain. This phenomenon illustrates the sensitivity of pressure shadows to changes in the nature of progressive deformation.

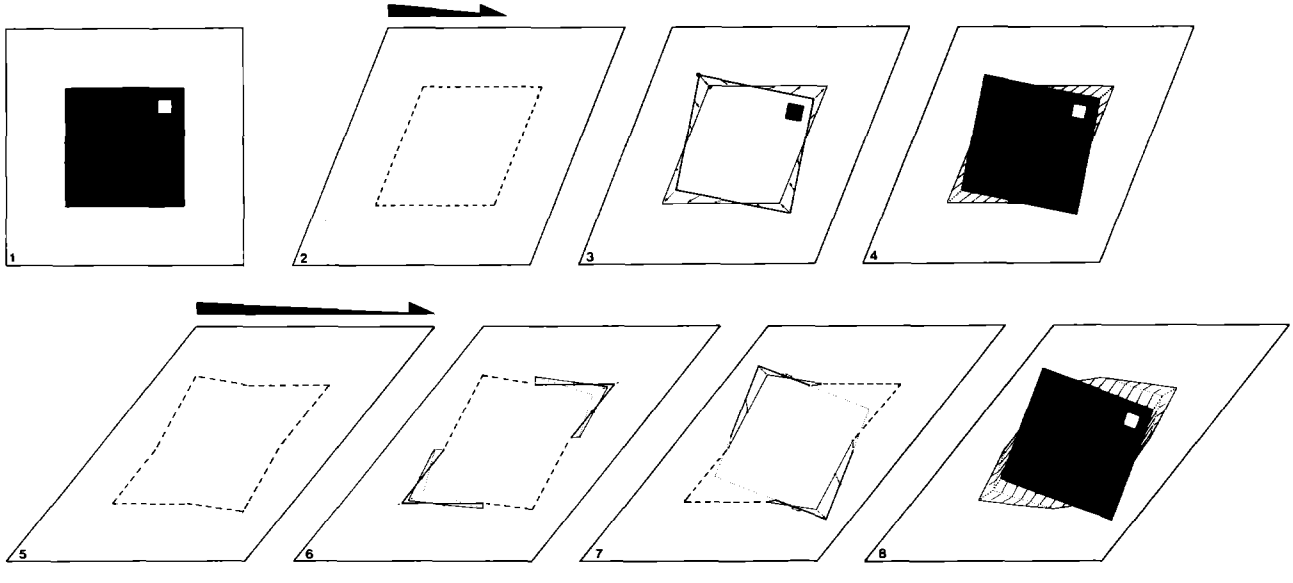

Fig. 4. Rigid-fibre model with displacement-controlled fibres. True increments of deformation are 5 times smaller than illustrated. (1) Initial configuration, showing object in black. (2) Homogeneous deformation of matrix. (3) First minimization, with remaining gaps and overlaps. (4) First incremental growth of pressure shadows. (5) Second homogeneous deformation of matrix. (6) Best fit between (i) external boundary of pressure shadows and (ii) matrix. (7) Best fit between (i) object boundary outside pressure shadows and (ii) matrix. (8) Second incremental growth of pressure shadows.

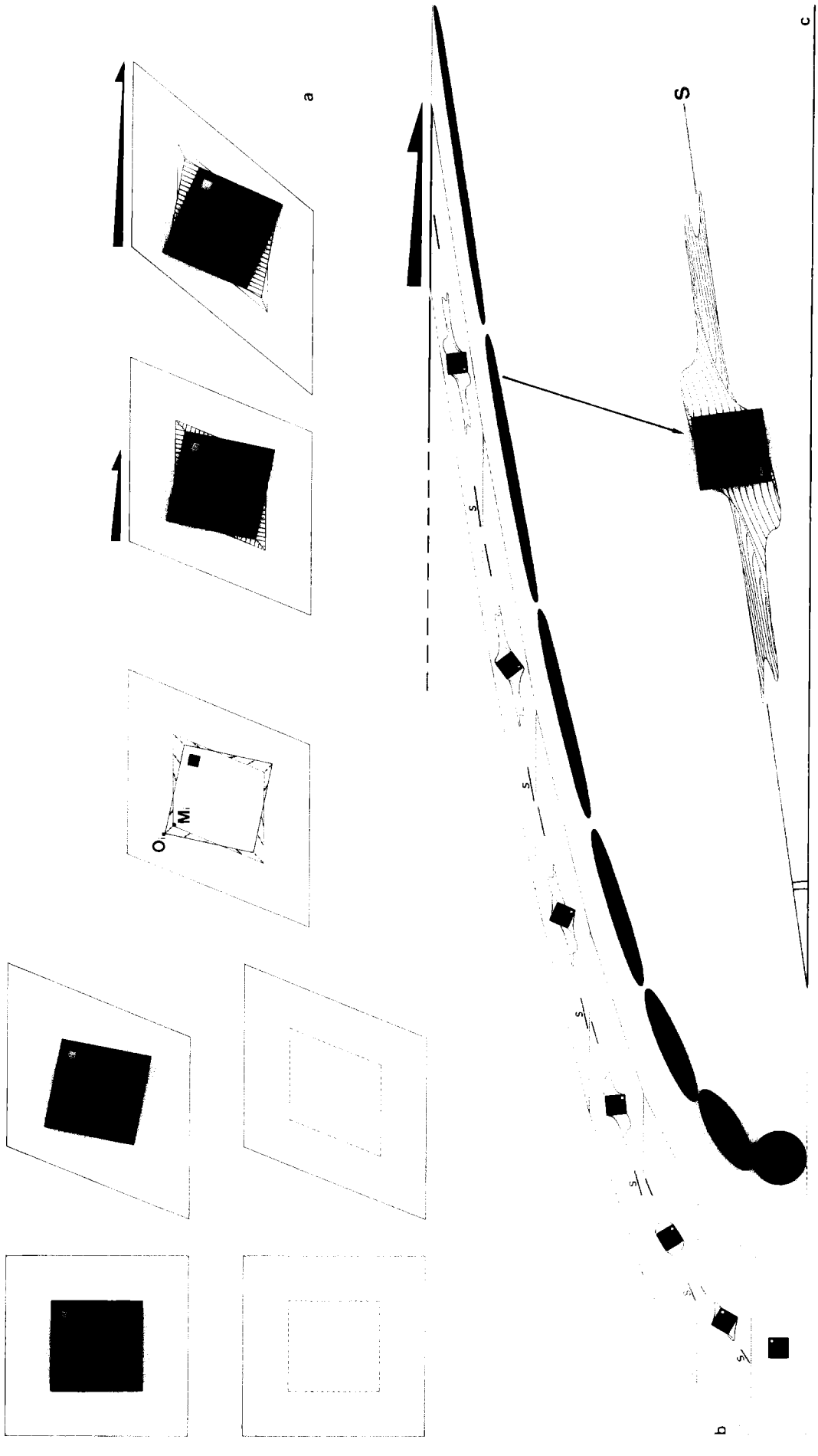

Fig. 5. Computer model for simple shear, where pressure shadow fibres are deformable and face-controlled. (a) Details of first few increments. (b) Results for successive amounts of shear ($\gamma = 0$–6), shown distributed across a shear-zone. Strain ellipses shown in black. (c) Detail of pressure shadow ($\gamma = 6$) showing fibres and suture lines.

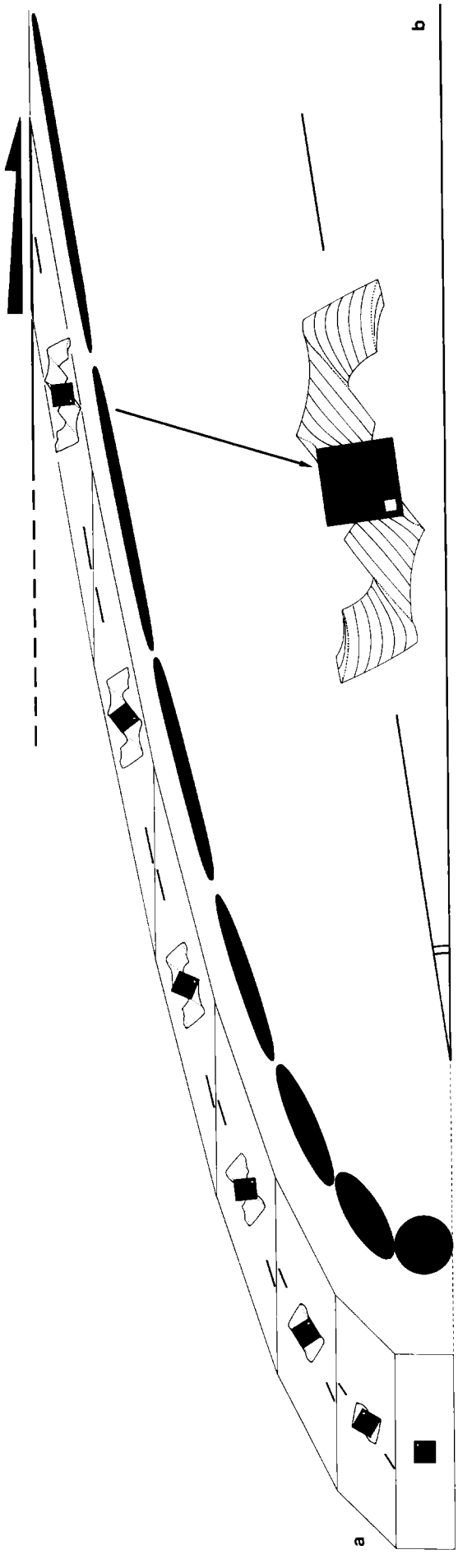

Fig. 6. Computer model for simple shear, where pressure-shadow fibres are rigid and displacement-controlled (a) Results for successive amounts of shear ($\gamma = 0$–6) shown distributed across a dextral shear zone. Strain ellipses shown in black. (b) Detail of pressure shadow ($\gamma = 6$) showing fibres and suture lines

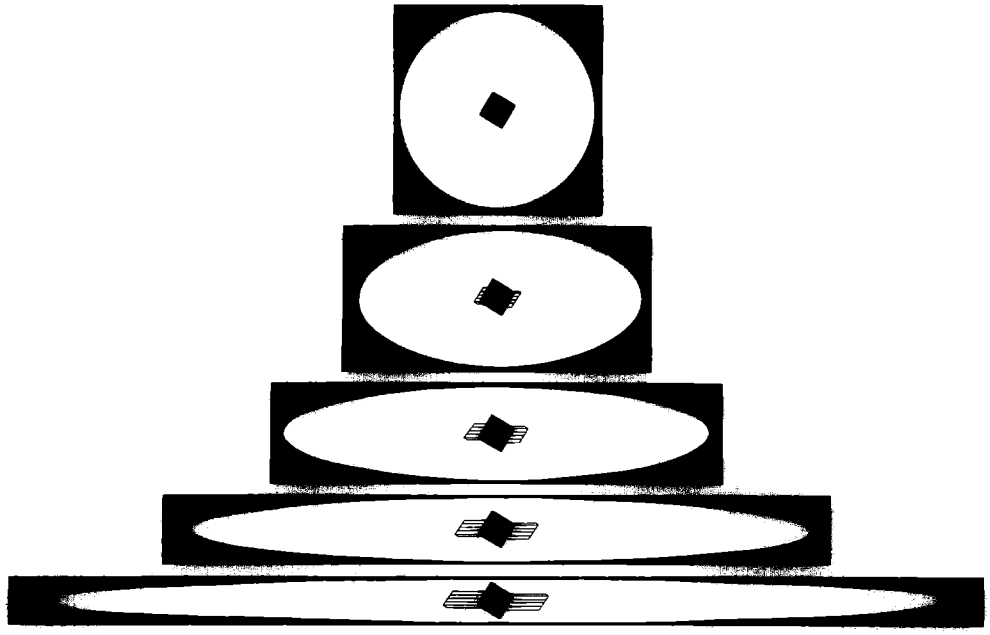

Fig. 7. Computer model for pure shear, where pressure shadow fibres are rigid and displacement-controlled. Notice that square object is oblique to bulk-strain axes

Example 4 (Fig. 12)

Geological setting. This framboidal pyrite (Figs. 1c and 12a) from Lagrave (French Alps), shows sigmoidal asymmetric pressure shadows made of quartz fibres. The thin section (Fig. 1c) is not exactly in the *XZ* plane and the pressure shadows appear thicker than the computed ones.

The model. A best fit is obtained using a rigid displacement-controlled fibre model (Fig. 12b). The parameters are: $\gamma_f = 3$, $\gamma_i = 0.1$, with no shortening or elongation (i.e. simple shear).

The asymmetry of pressure shadow and the pattern of fibres are indicative of a non-coaxial strain history.

Example 5

Geological setting. This sample (Fig. 13a) from Centuri (Northern Corsica), has undergone intense Alpine deformation under conditions of high-pressure and low-temperature metamorphism (Malavieille 1983).

The model. A best fit is obtained using deformable face-controlled fibres (Fig. 13b), and parameters: $\gamma_i = 0.1$, $\gamma_f = 4$, with no shortening or elongation (simple shear).

In the natural sample, the pressure shadows consist of weakly oriented large quartz crystals, with only a few fibres close to the pyrite and perpendicular to its margin. The tapered morphology of the pressure shadow, com-

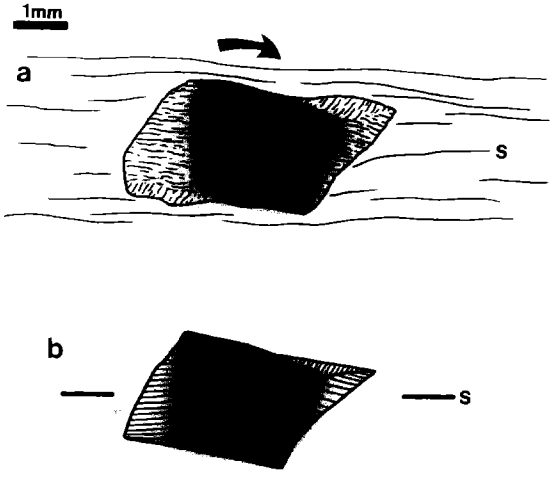

Fig. 8. Example 1. (a) comparison of a real pressure shadow (b) with computed pressure shadow. Model assumptions: deformable and face-controlled fibres; simple shear in increments of $\gamma_i = 0.1$, up to total of $\gamma_f = 1$; no shortening and no elongation. Black arrow indicates sense of rotation; S = cleavage surface.

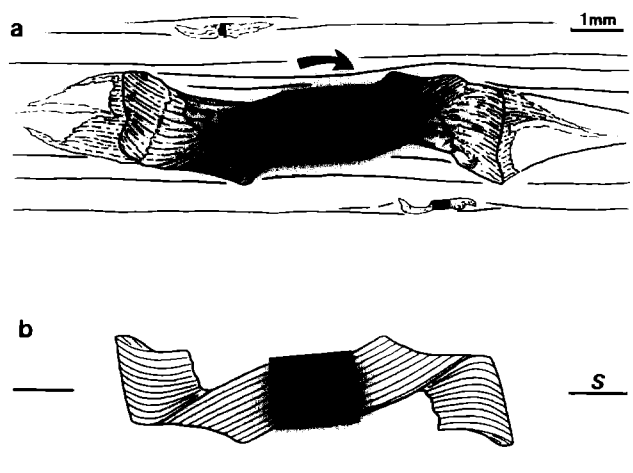

Fig. 9. Example 2. (a) Pressure shadow drawn from Fig. 1(a). (b) Computed pressure shadow with assumptions: rigid and displacement-controlled fibres; strain parameters $\gamma_i = 0.2$; $K_{f1} = 0.98$; $K_{f2} = 1/0.98$ (plane strain); finite-strain parameters $\gamma_f = 5$; $K_n = 5$; $K_{f1} = 0.6$; $K_{f2} = 1.66$.

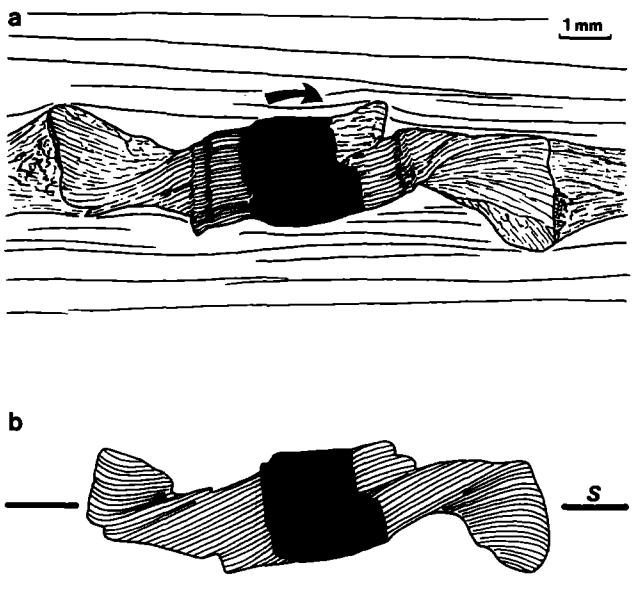

Fig. 10. Example 3. (a) Pressure shadow drawn from Fig. 1(b). (b) Computed pressure shadow using the same laws and parameters as in example 2.

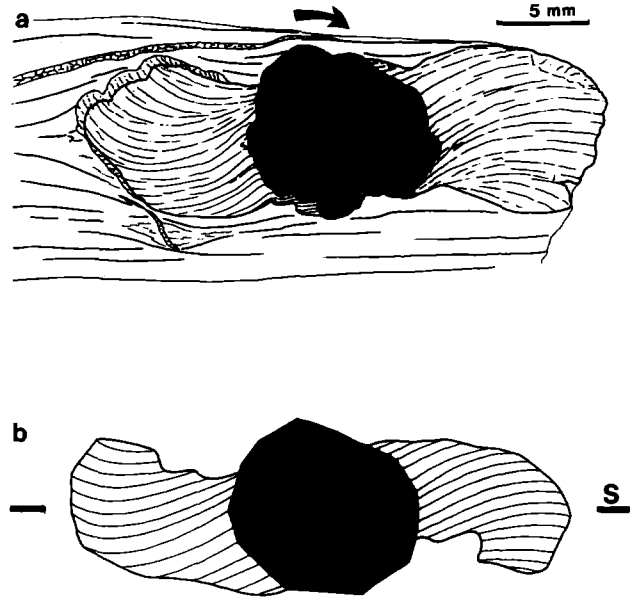

Fig. 12. Example 4.(a) Pressure shadow drawn from Fig. 1(c). (b) Computed pressure shadow, with assumptions: rigid and displacement-controlled fibres; strain parameters $\gamma_i = 0.1, \gamma_f = 3$, no shortening or elongation. (The thin section cut across this sample is not exactly perpendicular to the schistosity plane. That could explain that the actual pressure shadow morphology seems thicker than the computed one.)

pared with the previous example, shows how deformable it is.

SHEAR CRITERIA

The best criterion for determining the sense of shearing is the asymmetry of pressure shadows in XZ sections. This asymmetry is often well marked and pressure shadows may be S-shaped (Fig. 14). Unfortunately in slates it is dificult to observe good XZ sections, while it is often easier to observe the cleavage plane (XY). On the cleavage plane the shape around an asymmetric pressure shadow can be used to indicate the shear sense. The shear direction is from the hollow towards the hump (Fig. 15).

CONCLUSIONS

(1) From computer modelling, we suggest that pressure shadows may be used to estimate bulk strain and shear sense in deformed rocks.

(2) Asymmetry of pressure shadows may be used to infer a sense of shear in non-coaxial deformation.

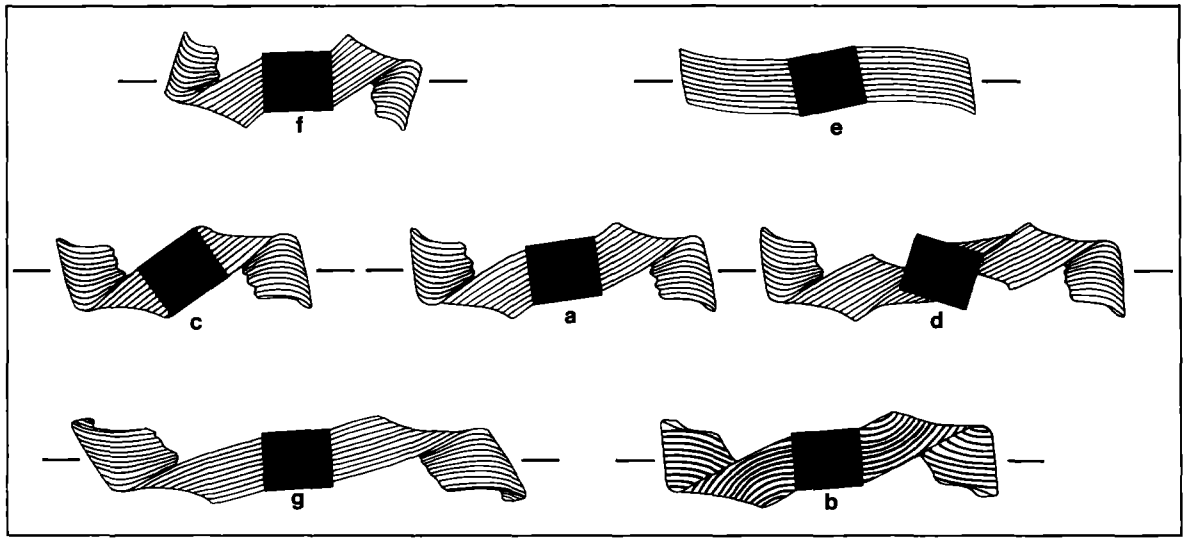

Fig. 11. Changes in simulated pressure-shadow shapes for example 2, using different laws and parameters. (a) As in Fig. 9(b); rigid and displacement-controlled fibres. (b) Face-controlled fibres with the same parameters. (c) and (d) Change in simple shear magnitude: (c), $\gamma_f = 4$; (d), $\gamma_f = 6$. (e) Pure shear only. (f) and (g) Change in the pure shear magnitude: (f), zero (simple shear); (g), $K_{il} = 0.96$ and $K_{if} = 2.77$.

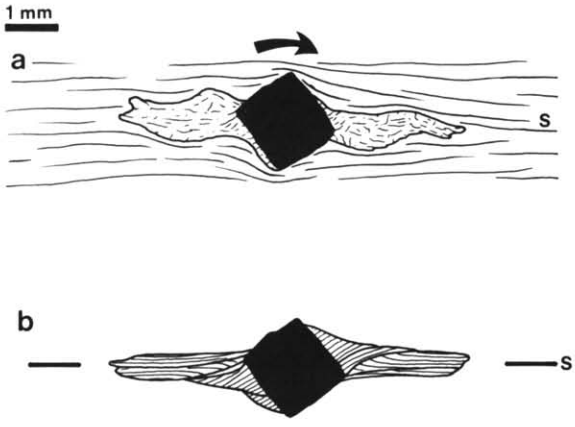

Fig. 13. Example 5: comparison of real pressure shadow (a) with computed pressure shadow. (b) Deformable- and face-controlled fibres; strain parameters, $\gamma_i = 0.1, \gamma_f = 4$, no flattening, shortening or elongation.

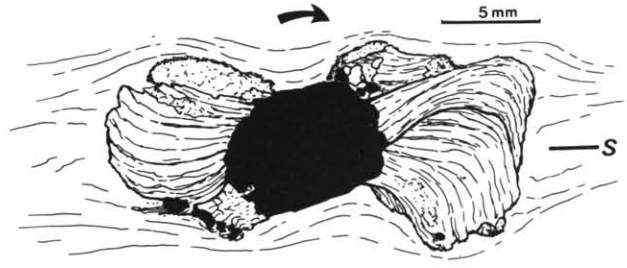

Fig. 14. Curved quartz pressure shadow around a framboidal pyrite from Lagrave (French Alps). The asymmetry indicates a dextral shear.

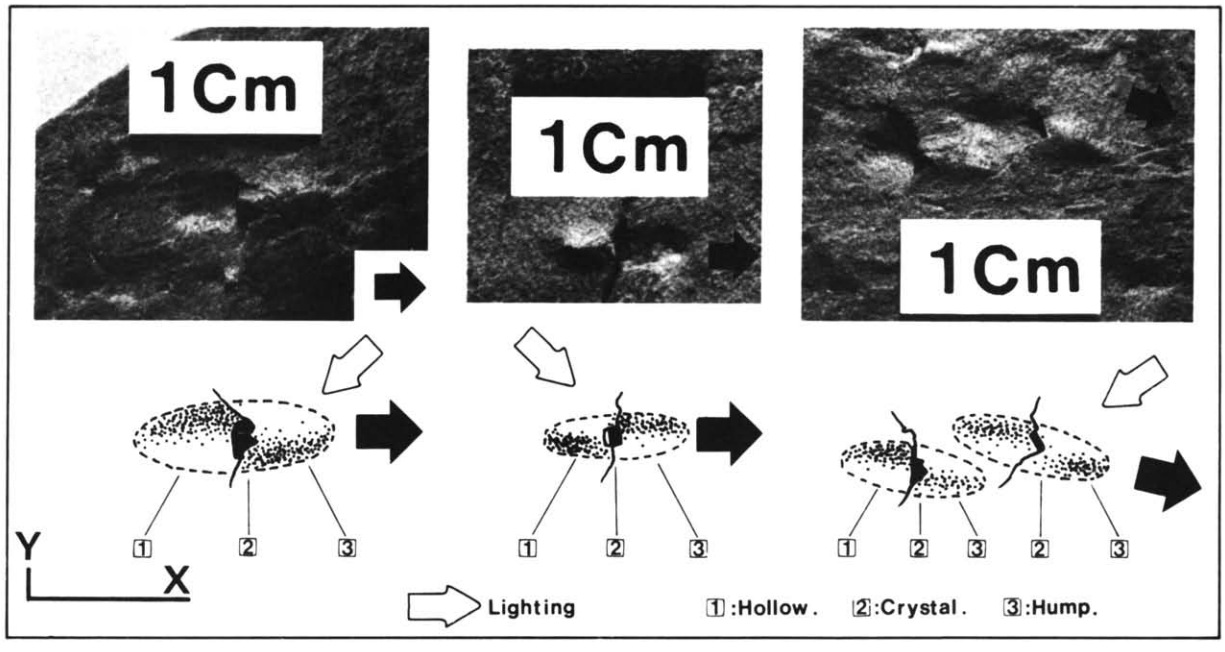

Fig. 15. Morphology of cleavage surfaces around rigid crystals, indicating the shear sense (black arrow) from the hollow towards the hump.

(3) The pressure shadow geometry is very sensitive to variations of deformation parameters.

(4) Distinct pressure-shadow patterns were simulated for the different cases of deformable and rigid fibres, in simple shear. Rigid fibres exhibit sinuous ribbon-like shadows, whereas deformable fibres show a gradually tapering form.

(5) The best-fit models to the natural examples were obtained from incremental strain parameters which did not change during the simulation. This suggests that the deformation increments varied only slightly, if at all, during the growth of these natural pressure shadows.

(6) The models illustrate the influence of crystallization laws on the geometry and internal structure of pressure shadows.

(7) On an interactive graphical display, a large number of pressure shadows can be rapidly computed. This makes the method useful for regional studies.

Acknowledgements—This work was funded by the U.A. 266 of C.N.R.S. Data processing and computing were done with the help of the C.U.T.I. and C.N.U.S.C. of Montpellier. Many thanks to M. Mattauer for stimulating discussions, to H. Echtler, J. L. Bonnetain, P. Cobbold and an anonymous reviewer for help with English and to J. Faure and M. F. Roch for typing the manuscript.

REFERENCES

Burg, J. P., Matte, Ph., Brunel, M., Andrieux, J., Li Tingdong, Chen Guoming, Li Guangcen & Xiao Xuchang, 1980. Présence et signification d'une phase de déformation antérieure au flysch à blocs, réputé d'âge crétacé supérieur, au sud de la suture du Tsangpo (Tibet méridional). In: *Mission Franco-Chinoise au Tibet.* Editions du C.N.R.S. (edited by Mercier, J. L. and Li Guangcen), 351–356.

Choukrone, P. 1971. Contribution à l'étude des mécanismes de la déformation avec schistosité grâce aux cristallisations syncinématiques dans les "zones abritées" ("pressure shadows"). *Bull. Soc. geol. Fr.* **13**, 257–271.

Demay, A. 1942. Microtectonique et tectonique profonde. *Mém. Serv. Carte géol. dét Fr.*

Durney, D. W. & Ramsay, J. G. 1973. Incremental strains measured by syntectonic crystal growths. In: *Gravity and Tectonics* (edited by De Jong, K. A. and Scholten, R.). Wiley, New York, 67–96.

Elliott, D. 1972. Deformation paths in structural geology. *Bull. Geol. Soc. Am.* **83**, 2621–2638.

Etchecopar, A. 1974. Simulation par ordinateur de la déformation progressive d'un agrégat polycristallin. Unpublished thèse 3ème cycle, Université de Nantes.

Etchecopar, A. 1977. A plane kinematic model of progressive deformation in a polycrystalline aggregate. Tectonophysics **39**, 121–139.

Etchecopar, A. 1984. Etude des états de contrainte en tectonique cassante et simulations de déformations plastiques (Approche mathématique). Unpublished thèse d'Etat. Université de Montpellier.

Fairbairn, H. W. 1950. Pressure shadows and relative movements in shear zones. *Trans. Am. Geophys. Union* **31**, 914–916.

Frankel, J. 1957. Abrated pyrite crystals from the Witwatersrand gold mines. *Mineralog. Mag.* **31**, 392–401.

Langheinrich, G. 1964. Vergleichende Untersuchungen über das Verhältnis der Schieferung zur Faltung unter Berücksichtigung des Stockwerk-problems. *Neues Jb. Geol. Paläont. Abh* **120**, 41–80.

Malavieille, J. 1983. Etude tectonique et microtectonique de la nappe de socle de Centuri (zone des schistes lustrés de Corse); conséquences pour la géométrie de la chaîne alpine. *Bull. Soc. geol. Fr.* **25**, 195–204.

Malavieille, J. Etchecopar, A. & Burg, J. P. 1982. Analyse de la géométrie des zones abritées: simulation et application à des exemples naturels. *C.r.Acad.Sci., Paris* **294**, 279–284.

Malavieille, J. & Etchecopar, A. 1984. Modélisation informatique et visualisation du développement des cristallisations en zones abritées: montage d'animation vidéo et applications géologiques. *Géochronique* **10**, 6.

Mügge, O. 1928. Uber die Entstehung faseringer Minerale und ihrer Aggregationsformen. *Neues Jb. Miner. Beil. Bed.* **58**, 303–348.

Mügge, O. 1930. Bewegungen von Porphyroblasten in Phylitten und ihre Messung. *Neues Jb. Miner. Geol. Palaeont. Abh.* **61**, 469–520.

Nicolas, A. 1984. *Principes de Tectonique*. Masson, Paris.

Pabst, A. 1931. "Pressure shadows" and the measurements of orientation of minerals in rocks. *Am. Miner.* **16**, 55–61.

Ramsay, J. G. 1967. *Folding and Fracturing of Rocks*. McGraw Hill, New York.

Ramsay, J. G. & Huber, M. I. 1983. *The Techniques of Modern Structural Geology; Volume* 1: *Strain Analysis*. Academic Press, New York.

Simpson, C. & S. M. Schmid. 1983. An evaluation of criteria to deduce the sense of movement in sheared rocks. *Bull. geol. Soc. Am.* **94**, 1281–1288.

Spry, A. 1969. *Metamorphic Textures*. Pergamon Press, Oxford.

Subieta, T. A. 1977. Analyse quantitative de la déformation dans un secteur de la zone externe des Alpes (La Javie—Nord-Est de Digne). Unpublished thèse 3ème cycle, Université de Montpellier.

White, S. H. & Wilson, C. J. L. 1978. Microstructure of some quartz pressure fringes. *Neues. Jb. Miner. Geol. Palaeont. Abh.* **134**, 33–51.

Zwart, H. J. & Oele, J. A. 1966. Rotated magnetite crystals from the Rocroi Massif (Ardennes). *Geologie Mijn.* **45**, 70–74.